Aalborg Universitet

Frequency Characteristics of Path Loss and Delay-Angular Profile of Propagation Channels in An Indoor Room Environment in SHF Bands

HANPINITSAK, Panawit; SAITO, Kentaro ; Fan, Wei; Takada, Jun-ichi; Pedersen, Gert F.

Published in:
TECHNICAL REPORT OF IEICE

Publication date:
2017

Document Version
Accepted author manuscript, peer reviewed version

Link to publication from Aalborg University

Citation for published version (APA):
HANPINITSAK, P., SAITO, K., Fan, W., Takada, J., & Pedersen, G. F. (2017). Frequency Characteristics of Path Loss and Delay-Angular Profile of Propagation Channels in An Indoor Room Environment in SHF Bands. In *TECHNICAL REPORT OF IEICE* (481 ed., Vol. 116, pp. 153-158). The Institute of Electronics, Information and Communication Engineers.

General rights
Copyright and moral rights for the publications made accessible in the public portal are retained by the authors and/or other copyright owners and it is a condition of accessing publications that users recognise and abide by the legal requirements associated with these rights.

- Users may download and print one copy of any publication from the public portal for the purpose of private study or research.
- You may not further distribute the material or use it for any profit-making activity or commercial gain
- You may freely distribute the URL identifying the publication in the public portal -

Take down policy
If you believe that this document breaches copyright please contact us at vbn@aub.aau.dk providing details, and we will remove access to the work immediately and investigate your claim.

Downloaded from vbn.aau.dk on: May 17, 2025

社団法人　電子情報通信学会
THE INSTITUTE OF ELECTRONICS,
INFORMATION AND COMMUNICATION ENGINEERS

信学技報
TECHNICAL REPORT OF IEICE.

Frequency Characteristics of Path Loss and Delay-Angular Profile of Propagation Channels in An Indoor Room Environment in SHF Bands

Panawit HANPINITSAK†, Kentaro SAITO†, Wei FAN††, Jun-ichi TAKADA†, and Gert FRØLUND PEDERSEN††

† Department of Transdiciplinary Science and Engineering
School of Environment and Society, Tokyo Institute of Technology
S6–4, 2–12–1, O-okayama, Meguro-ku, Tokyo, 152–8550, Japan
†† Department of Electronic Systems, Faculty of Engineering and Science
Aalborg University, DK-9220, Aalborg, Denmark
E-mail: †{hanpinitsak@ap.ide.titech.ac.jp,saitouken@tse.ens.titech.ac.jp,takada@ide.titech.ac.jp},
††{wfa@es.aau.dk,gfp@es.aau.dk}

Abstract Comparison of channel characteristics at many frequency bands is necessary to study the frequency-dependency which is important for consistent multi-frequency spatial-temporal channel model. Path loss (PL) and power spectrum characteristics of the channel measured in a typical classroom line-of-sight (LOS) were presented at three different bands: 3, 10 and 28 GHz. The results showed that diffuse scattering was more significant in lower bands, whereas specular reflection was more significant in higher bands. Moreover, PL of 3 and 10 GHz were higher than their free space PL (FSPL) counterparts. For 28 GHz band, the PL was roughly the same as FSPL.

Key words Beam forming, Indoor environments, Microwave propagation, Millimeter wave propagation, Propagation losses

1. Introduction

Because of the substantial increase in the mobile data traffic in recent years, the 5th generation (5G) wireless system has been researched extensively [1][2]. To accommodate the vast amount of traffic, 5G is targeting frequency bands higher than 10 GHz which can provide large bandwidth. Furthermore, massive number of antenna is planned to be utilized to send massive number of multiple streams simultaneously. Most researchers have been focusing on 60 GHz band due to its high priority. However, 28 GHz band has also been potential candidate and has been extensively investigated recently [3–6]. Even though it is intended that high frequency system will be deployed in the 5G system, the “fall-back" alternatives in which the system can switch to lower frequency bands is essential due to many uncertainties of the high frequency bands such as sensitivity to blockage and rapid mobile station (MS) movement [7]. Therefore, for system design of the wireless systems with high robustness and reliability, it is necessary to characterize the channel not only at high frequency bands, but also at lower bands. Thus, some researchers have been starting to focus on analysing the frequency-dependency channels in many different frequency bands in the same environment [3,8–12]. To the authors' best knowledge, in indoor cases, the frequency-dependency analysis is still limited with most papers comparing the power spectrum and delay spread between different bands.

In this paper, the path loss (PL) and power-angle-delay profile (PADP) of the channels in an indoor, line-of-sight (LOS) classroom environment is presented and discussed at three different bands: 3, 10 and 28 GHz. All three bands have 2 GHz bandwidth. The beamforming (BF) is used to obtain the PADP [13], whereas the power sum of the impulse response is calculated to find the PL of each transmitter (Tx) location [14]. The comparison results showed that more multipaths can be observed at lower bands due to diffuse scattering effect. The PL comparison with free space PL (FSPL) and PL fit using power law model indicated that the PL of 3 and 10 GHz bands are higher than FSPL due to wave guiding effect in a small room, whereas the PL of 28 GHz band is roughly the same as FSPL, indicating that the wave guiding effect is negligible. Moreover, since the wave guiding effect at lower bands is stronger, the PL exponent (PLE) is smaller in those bands.

The rest of the paper is organized as follows: In Section 2, the radio channel measurement is explained. Section 3

briefly describes the BF and PL calculation steps. After that, Section 4 presents the BF and PL analysis results. Finally, Section 5 summarizes the findings of this paper and provides the future work.

2. Virtual Array Radio Channel Measurement Method

In this paper, the virtual uniform circular array (UCA) system [8,9] was utilized for the radio channel measurement. The simplified system is shown in Fig. 1. This system consist of five main parts: the vector network analyzer (VNA), LO/IF distribution unit to divide the local oscillator (LO) signal to mixers, test and reference mixers to down convert the received and transmitted signal to intermediate frequency (IF) signal, and the automatic rotator to rotate the antenna after each measurement sweep [8, 9]. The single-input, single-output (SISO) channel transfer function at the i-th Rx location ($\boldsymbol{H}_i$) was calculated by the ratio between the IF signal down converted from the Rx and Tx signal. The single-input, multiple-output (SIMO) channel transfer functions for all elements of UCA were realized virtually by rotating the automatic rotator which is connected to the external trigger port of the vector network analyzer (VNA) as shown in Fig. 1. Firstly, the rotator sends out the trigger to VNA to make it sweeps. After the VNA finish sweeping, it sends trigger to the rotator to rotate to the new position. After the rotator rotates to the new position, it sends trigger to VNA to make it sweeps again. This process was repeated until the rotator rotates to all the Rx antenna locations. Thus, the SIMO channel transfer function was calculated from SISO channel transfer function as follows

$$\boldsymbol{H} = [\boldsymbol{H}_0, \boldsymbol{H}_1, ..., \boldsymbol{H}_i, ..., \boldsymbol{H}_{I-1}] \tag{1}$$

where I, $\boldsymbol{H}_i$ are the number of Rx antenna locations, channel transfer function at i-th Rx location, respectively.

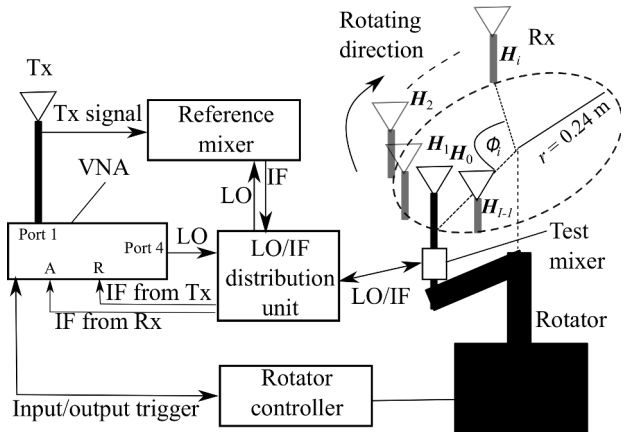

Fig. 1: Virtual UCA system

3. Beamforming and Pathloss Calculation Methods

3. 1 Beamforming

For simplicity, this paper utilized the BF [13] to estimate the PADP of the channel. In the first step, the array frequency response of the channel was calculated by

$$Y(f,\phi) = \frac{1}{I}\sum_{i=0}^{I-1} H_i(f)\exp(-\mathrm{j}2\pi f(r/c)\cos(\phi-\phi_i)) \tag{2}$$

where f, $H_i(f)$, r, ϕ, ϕ_i, and c are the carrier frequency, frequency transfer function at i-th Rx location and at carrier frequency f, radius of UCA, angle-of-arrival (AoA) of the BF, angle of the i-th Rx antenna location, and speed of light, respectively.

After that, the array impulse response (IR) was obtained by using inverse discrete Fourier transform (IDFT) of this array frequency response.

$$y(\tau,\phi) = \sum_{k=0}^{N-1} Y(f_k,\phi)\exp(\mathrm{j}2\pi f_k\tau) \tag{3}$$

where N, f_k and τ are the number of frequency bins, the frequency of the k-th frequency bin, and delay, respectively.

Finally, the PADP was calculated by taking the absolute and square of this array impulse response.

3. 2 Path Loss Calculation

There are 2 steps for PL calculation for each measurement snapshot, which is similar to the calculation in [14]. To reduce the effect of large variation of antenna gain across the wide bandwidth, the PL was calculated only for 400 MHz bandwidth (150 frequency bins) around the center frequency of each band. In the first step, assuming that the paths are concentrated in the azimuth plane, the antenna gain de-embedded IR of the i-th antenna element was calculated by

$$h_i[n] = \frac{1}{N}\sum_{k=0}^{N-1} \frac{H_i[k]}{(G_{\mathrm{Tx}}[k]G_{\mathrm{Rx}}[k])^{1/2}}\exp(j2\frac{\pi}{N}kn) \tag{4}$$

where $H_i[k]$, $G_{\mathrm{Tx}}[k]$, $G_{\mathrm{Rx}}[k]$, n denote the channel transfer function, Tx and Rx gain at the k-th frequency bin, and delay bin respectively. i is the array element index. Then, PL was calculated by

$$\mathrm{PL} = \left(\frac{1}{I}\sum_{i=0}^{I-1}\sum_{n\in\mathcal{U}}|h_i[n]|^2\right)^{-1} \tag{5}$$

where $\mathcal{U}$ is the set of delay bins in which the power is above the noise level. In case of 3 and 10 GHz, all 150 delay bins were used for the PL calculation. For 28 GHz, the first 75 bins and last 30 bins were used.

4. Results and Discussion

4.1 Measurement Environment and Channel Sounder Specification

The radio channel measurement was conducted in a typical small class room in Aalborg University, Aalborg, Denmark. The classroom environment with Tx and Rx locations, and measurement photographs are shown in Fig. 2 and 3, respectively. Three sides of the room are covered by the concrete walls. The window frames are made from metal and the glass is the energy efficient glass covered with thin metallic layer. The transmitter (Tx) is a single commercial wideband biconical antenna and the Rx is a virtual 360 elements UCA with the radius of 0.24 m utilizing the modified biconical antenna [15]. There are five rows of tables with the height of 0.74 m. The measurement setup parameters are depicted in Table 1. A total of 20 spatial snapshots were measured by moving the Tx between the tables. Each Tx in each row was spaced 80 cm apart. Both Tx and Rx were mounted at 1.5 m height.

Table 1: Channel sounder specification

Parameters	Values
Center frequency	3, 10, 28 GHz
Bandwidth	2 GHz
Tx antenna	Commercial biconical antenna (A-INFO SZ-2003000)
Rx antenna	Modified biconical antenna [15]
Number of Rx elements	360
UCA radius	0.24 m
Number of frequency bins	750
Maximum delay	375 ns
Tx and Rx height	1.5 m

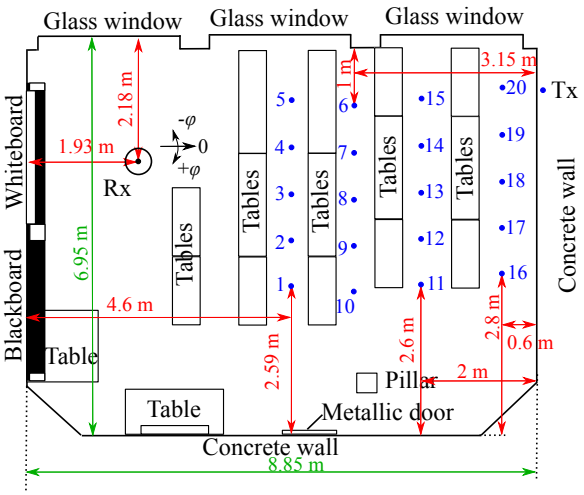

Fig. 2: Floor plan with Tx and Rx locations

4.2 Delay-Angle Power Spectrum Comparison

Figs. 4, 5 and 6 (a) shows the PADP results at the third, seventh and twelfth Tx location in which the locations are depicted in Fig. 2. The paths were visually identified and numbered from peaks of PADP and the results were plotted in Figs. 4, 5 and 6 (b) for the third, seventh and twelfth Tx location respectively. From these results it could be seen that PADP suffered from joint angular-delay sidelobe especially the LOS component and strong specular reflected path due to the wide bandwidth and large array size used, which was also observed in [8, 13]. In case of 3 GHz band, the floor and table reflected paths could be seen as shown in Fig. 4 and 5 due to the wide elevation beamwidth. Moreover, more multipaths were detected due to diffuse scattering effect. This effect is from the paths scattered from the small objects in the environment, which is stronger in lower frequency bands. On the other hand, the channels in 10 and 28 GHz bands were sparse and dominated by the specular reflection due to much smaller wavelength. These results also agree with the results in [8] which utilize almost the same measurement system and antennas.

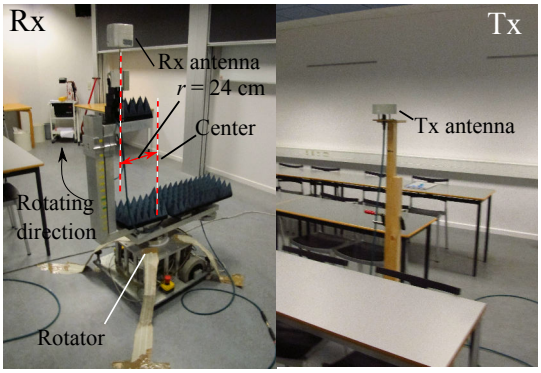

Fig. 3: Photo of the measurement

4.3 Path Loss Comparison and Model Fitting

Fig. 7 shows the measured PL compared with the FSPL at the center frequency of each band. As expected, the measured PL at 3 and 10 GHz were smaller than the FSPL in LOS scenario because of the wave guiding effect of a small room, which was similarly observed in [14]. On the other hand, in case of 28 GHz band, the measured PL was roughly the same as FSPL. This is because the LOS component was much more dominant at higher frequency bands, whereas diffuse scattering and specular reflections were more dominant in the lower bands.

Fig. 8 and Table 2 show the power law model PL fitting results and the PL model parameters of all three bands, in which the PL is expressed by

$$\mathrm{PL[dB]} = a \cdot 10\log_{10}(d[\mathrm{m}]) + b + X \qquad (6)$$

where a and b represent the PLE and PL at 1 m distance, respectively. X is the shadowing variation, which is represented by the log-normal random variable with mean and

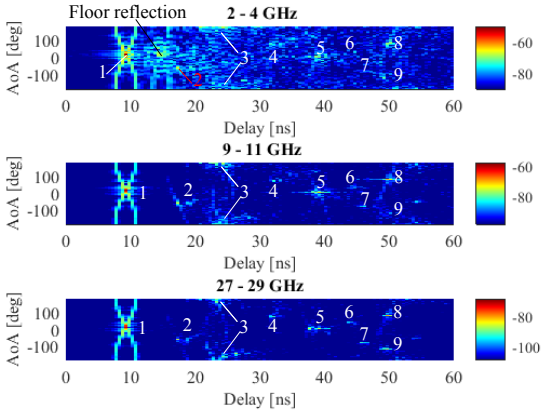

(a)

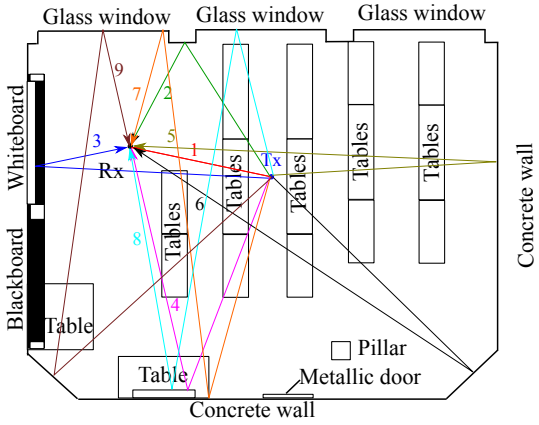

(b)

Fig. 4: PADP and identified paths at the 3-rd Tx location ((a) PADP, (b) paths identification).

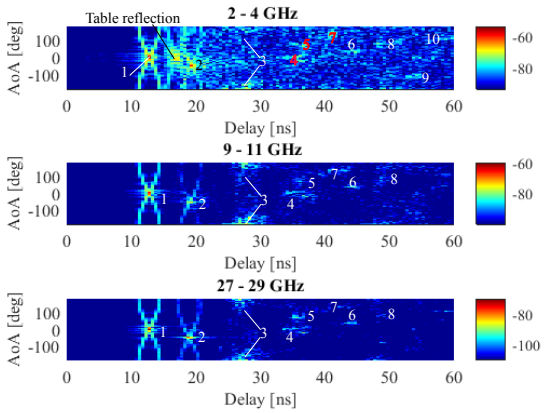

(a)

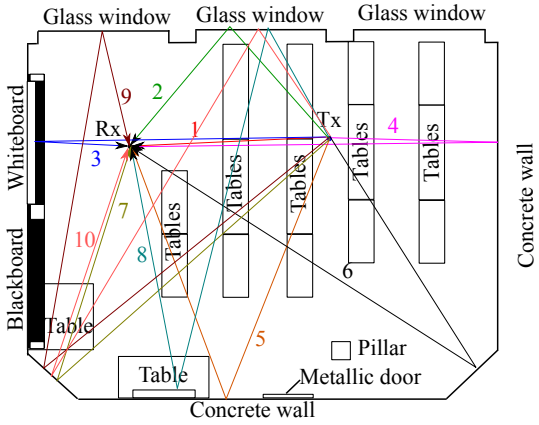

(b)

Fig. 5: PADP and identified paths at the 7-th Tx location ((a) PADP, (b) paths identification).

variance equal to 0 and σ^2 respectively.

From these results, it could be seen that the PLE of all three bands were smaller than 2 and increases as the frequency increases. This was also due to the stronger wave guiding effect at lower frequency bands. In particular, the 3 GHz had much smaller PLE than the other two bands. One possible explanation is that the strong reflection and diffuse scattering from the concrete wall at the back of the room occurred at larger distances (Tx16-Tx20) since the Tx was very close to the wall. These results contradict to the results in [3, 12] which reported that the PLE decreases with frequency and is higher than 1.5. The possible explanation is that the size of the rooms in [3, 12] were much larger than the class room in this paper and hence the effect of the wave guiding was smaller. Moreover, both papers also measured the channel at larger Tx-Rx distances and have more spatial snapshots.

5. Conclusion

This paper presented the delay-angle power spectrum and

Table 2: Path loss model parameters

Frequency band (GHz)	a	b	σ
3	0.886	45.25	0.485
10	1.183	54.05	0.478
28	1.300	64.54	0.309

PL characteristics of channels in an indoor classroom environment using three SHF bands: 3, 10 and 28 GHz. The channels were measured using the VNA-based channel sounder and rotator to realize virtual UCA. The power spectrum results indicated that the diffuse scattering dominated the lower 3 GHz band and thus more multipaths could be observed, whereas the specular reflection was more significant in 10 and 28 GHz bands. The PL results showed that, as the result of the guiding effect of the small environment in lower bands, the measured PL at 3 and 10 GHz were few dBs lower than the FSPL counterparts and the PLE increased with frequency. In contrast, the measured PL at 28 GHz was almost equal to the FSPL because LOS dominates the channel. These results implied that, in case of small class room environment, the channel characteristics

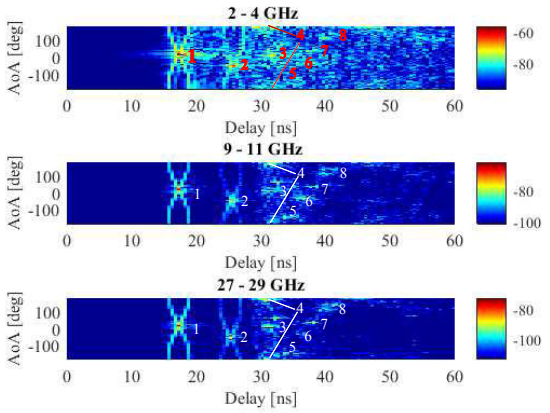

(a)

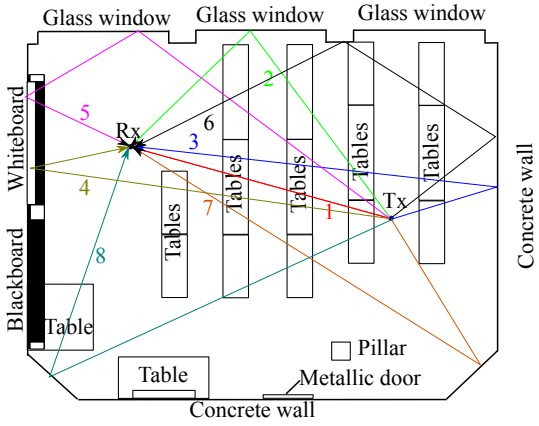

(b)

Fig. 6: PADP and identified paths at the 12-th Tx location ((a) PADP, (b) paths identification).

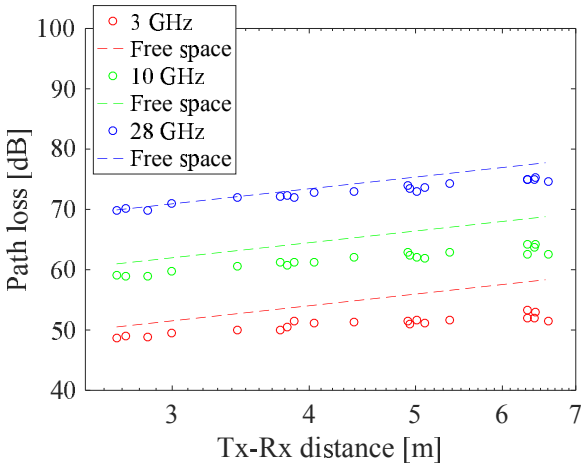

Fig. 7: Path loss comparison with free space path loss

vary significantly across the SHF bands. It is to be noted that the results presented here is specific to the class room environment. Thus, as the future work, it is also necessary to investigate the PADP and PL characteristics carefully in various types of environment. The influence of the antenna pattern on PL characteristics will also be more carefully analyzed. Moreover, the frequency dependent PL will be fitted and analyzed and the multipath will be resolved by using some sidelobe suppression techniques along with the parameter estimation algorithm [16].

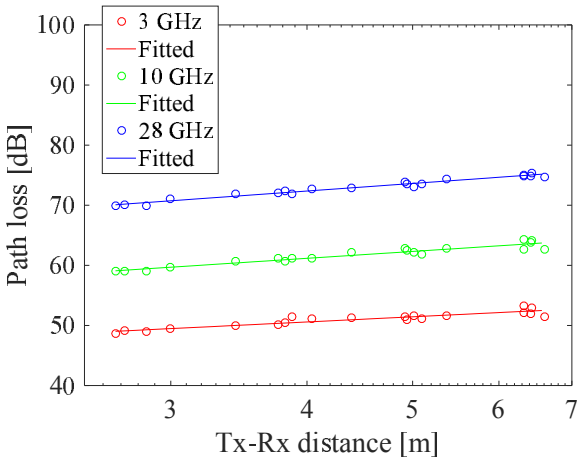

Fig. 8: Path loss model parameters fitting results

References

[1] K. Sakaguchi, E. M. Mohamed, H. Kusano, M. Mizukami, S. Miyamoto, R. E. Rezagah, K. Takinami, K. Takahashi, N. Shirakata, H. Peng, T. Yamamoto, and S. Nanba, "Millimeter-wave wireless LAN and its extension toward 5G heterogeneous networks," *IEICE Trans. on Commun.*, vol. E98-B, no. 10, pp. 1932–1948, July 2015.

[2] T. S. Rappaport, S. Sun, R. Mayzus, H. Zhao, Y. Azar, K. Wang, G. N. Wong, J. K. Schulz, M. Samimi, and F. Gutierrez, "Millimeter wave mobile communications for 5G cellular: It will work!" *IEEE Access*, vol. 1, pp. 335–349, 2013.

[3] G. R. Maccartney, T. S. Rappaport, S. Sun, and S. Deng, "Indoor office wideband millimeter-wave propagation measurements and channel models at 28 and 73 GHz for ultra-dense 5G wireless networks," *IEEE Access*, vol. 3, pp. 2388–2424, 2015.

[4] M. Lei, J. Zhang, T. Lei, and D. Du, "28-ghz indoor channel measurements and analysis of propagation characteristics," in *2014 IEEE 25th Annual International Symposium on Personal, Indoor, and Mobile Radio Communication (PIMRC)*, Sept 2014, pp. 208–212.

[5] X. Wu, Y. Zhang, C. X. Wang, G. Goussetis, e. H. M. Aggoune, and M. M. Alwakeel, "28 GHz indoor channel measurements and modelling in laboratory environment using directional antennas," in *2015 9th European Conference on Antennas and Propagation (EuCAP)*, May 2015, pp. 1–5.

[6] J. Lee, J. Liang, J. J. Park, and M. D. Kim, "Directional path loss characteristics of large indoor environments with 28 GHz measurements," in *2015 IEEE 26th Annual International Symposium on Personal, Indoor, and Mobile Radio Communications (PIMRC)*, Aug 2015, pp. 2204–2208.

[7] K. Haneda, "Channel models and beamforming at millimeter-wave frequency bands," *IEICE Trans. on Commun.*, vol. E98-B, no. 5, pp. 755–772, May 2015.

[8] W. Fan, I. Carton, J. Ø. Nielsen, K. Olesen, and G. F. Pedersen, "Measured wideband characteristics of indoor channels at centimetric and millimetric bands," *EURASIP Journal on Wireless Communications and Networking*, vol. 2016, no. 1, p. 58, 2016.

[9] J. Hejselbaek, W. Fan, and G. F. Pedersen, "Ultrawideband vna based channel sounding system for centimetre and mil-

limetre wave bands," in *2016 IEEE 27th Annual International Symposium on Personal, Indoor, and Mobile Radio Communications (PIMRC)*, Sept 2016, pp. 1–6.

[10] J. Medbo, N. Seifi, and H. Asplund, "Frequency dependency of measured highly resolved directional propagation channel characteristics," in *European Wireless 2016; 22th European Wireless Conference*, May 2016, pp. 1–6.

[11] K. Haneda, J. Järveläinen, A. Karttunen, M. Kyrö, and J. Putkonen, "Indoor short-range radio propagation measurements at 60 and 70 GHz," in *The 8th European Conference on Antennas and Propagation (EuCAP 2014)*, April 2014, pp. 634–638.

[12] M. Sasaki, M. Inomata, W. Yamada, N. Kita, T. Onizawa, and M. Nakatsugawa, "Path loss characteristics at multiple frequency bands from 0.8 to 37 GHz in indoor office," in *2016 10th European Conference on Antennas and Propagation (EuCAP)*, April 2016, pp. 1–4.

[13] C. Gentile, A. J. Braga, and A. Kik, "A comprehensive evaluation of joint range and angle estimation in indoor ultra-wideband location systems," *EURASIP Journal on Wireless Communications and Networking*, vol. 2008, no. 1, p. 248509, 2008.

[14] M. Kim, Y. Konishi, Y. Chang, and J. i. Takada, "Large scale parameters and double-directional characterization of indoor wideband radio multipath channels at 11 GHz," *IEEE Transactions on Antennas and Propagation*, vol. 62, no. 1, pp. 430–441, Jan 2014.

[15] S. S. Zhekov, A. Tatomirescu, and G. F. Pedersen, "Modified biconical antenna for ultrawideband applications," in *2016 10th European Conference on Antennas and Propagation (EuCAP)*, April 2016, pp. 1–5.

[16] B. Fleury, M. Tschudin, R. Heddergott, D. Dahlhaus, and K. Ingeman Pedersen, "Channel parameter estimation in mobile radio environments using the SAGE algorithm," *IEEE J. Select. Areas Commun.*, vol. 17, no. 3, pp. 434–450, Mar 1999.